

We are IntechOpen, the world's leading publisher of Open Access books Built by scientists, for scientists

6,900

Open access books available

186,000

International authors and editors

200M

Downloads

Our authors are among the

154

Countries delivered to

TOP 1%

most cited scientists

12.2%

Contributors from top 500 universities



WEB OF SCIENCE™

Selection of our books indexed in the Book Citation Index
in Web of Science™ Core Collection (BKCI)

Interested in publishing with us?
Contact book.department@intechopen.com

Numbers displayed above are based on latest data collected.
For more information visit www.intechopen.com



Finite Element Analysis to Study Percutaneous Heart Valves

Silvia Schievano, Claudio Capelli, Daria Cosentino,
Giorgia M. Bosi and Andrew M. Taylor
*UCL Institute of Cardiovascular Science, London
UK*

1. Introduction

Percutaneous valve implantation is an innovative, successful alternative to open-heart surgery for the treatment of both pulmonary and aortic heart valve dysfunction (Bonhoeffer et al., 2000; Cribier et al., 2002; Leon et al., 2011; Lurz et al., 2008; McElhinney DB et al., 2010; Rodes-Cabau et al., 2010; Smith et al., 2011; Vahanian et al., 2008). However, this minimally-invasive procedure still presents limitations related to device design: stent fracture, availability to a limited group of patients with very specific anatomy and conditions, and positioning and anchoring issues (Delgado et al., 2010; Nordmeyer et al., 2007; Schievano et al., 2007a). Computational simulations (Taylor & Figueroa, 2009), together with advanced cardiovascular imaging techniques can be used to help understand these limitations in order to guide the optimisation process for new device designs, to improve the success of percutaneous valve implantation, and ultimately to broaden the range of patients who could benefit from these procedures.

In this Chapter, we review the applications of finite element (FE) analyses to study percutaneous heart valve devices. The current percutaneous pulmonary valve implantation (PPVI) device is first presented: FE analyses were used to understand stent fractures in the patient specific setting and to study a potential solution to this problem. The shortcomings of the present PPVI stent have created a need for the next generation device. The optimisation study performed on this device using FE analyses, together with the first-in-man clinical application are described. The last part of this Chapter focuses on transcatheter aortic valve implantation (TAVI) and the innovative use of FE analyses to model patient specific implantation procedures. Computational analyses were used as a tool to assess the feasibility and safety of TAVI in patients who are currently considered unsuitable for this procedure.

2. Percutaneous pulmonary valve implantation

In the late 1990's, Professor Philipp Bonhoeffer developed a new technique of heart valve replacement that avoided the need for surgery (Bonhoeffer et al., 2000). This was based on the concept that a heart valve sewn inside a stent could be reduced in size, by crimping it onto a balloon catheter, and then introduced through a peripheral vessel to the desired

implantation site in the heart (Fig. 1). Inflation of the balloon deployed the valved stent and anchored it within the old dysfunctional valve. Over the last 11 years, this simple technique has shown a marked learning curve with safety and efficacy improvements that have led to CE mark in 2006, Food and Drug Administration (FDA) approval in 2010, and successful, worldwide clinical use of this procedure in the pulmonary position (>2,000 implants to date) and thousands of implants in the aortic position.

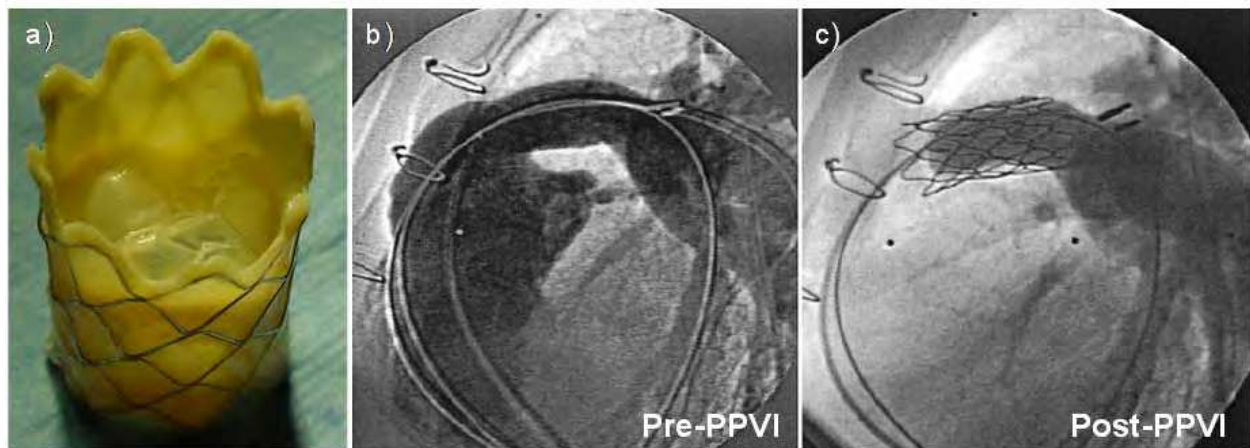


Fig. 1. a) Current PPVI device: Melody™, Medtronic, MN USA. Pulmonary angiograms b) pre- and c) post-PPVI in a patient. In this patient significant pulmonary regurgitation (contrast in the anterior right ventricle in b) has been completely abolished

2.1 Current device

The current PPVI device (Melody™, Medtronic, MN, USA) is constructed with a valve from a bovine jugular vein, sewn into a balloon-expandable, platinum-10% iridium stent (Fig. 1a). The stent is created by 6 wires, formed into a zig-zag shaped pattern, and welded together. Since the platinum welds were prone to fracture, this component of the PPVI was modified during the early clinical experience by introducing a gold braising process to reinforce the crowns. The bovine vein is attached to the stent by sutures around the proximal and distal rings and at each strut intersection. Bovine jugular venous valves are available only up to 22 mm of diameter, thus limiting the use of this minimally-invasive technique to those patients who have a small implantation site. During the procedure in the catheterisation laboratory, the valved stent assembly is hand-crimped to a size of 6 mm onto a custom made delivery system, before being re-expanded inside the patient's implantation site.

2.1.1 Understanding and predicting stent fractures

During the development phases of the current PPVI device, simple bench and animal experiments were performed as part of routine preclinical testing. These *in-vitro* and *in-vivo* experiments predicted valve degeneration with no stent fracturing. However, in our clinical practice, the opposite occurred – good valve function, ~20% stent fractures (Nordmeyer et al., 2007). These discrepancies were most likely due to the fact that in patients, the *in-vivo* loading conditions could not be correctly reproduced with experimental set-ups, where the boundary conditions are simplified and not representative of the real situation. For example, in the bench experiments for fatigue assessment, PPVI stents were placed in distensible

cylindrical tubes. However, the final shape of the PPVI stent *in situ* is a long way away from being uniformly cylindrical.

In order to better understand and predict the stent mechanical performance and durability, the implantation site morphology has to be included into *in-vitro* testing. To demonstrate this concept, and to test that computational analysis can indeed predict where stent fractures will occur, we reproduced patient-specific procedures using computational analysis.

Five patients (I to V) who underwent PPVI and experienced fracture between 1 and 6 months after implantation were selected (Cosentino et al., 2011). Biplane, orthogonal, fluoroscopy images (Axiom Artis Flat Detector system, Siemens Medical Systems, Germany) from the actual PPVI procedures of these patients were used to reconstruct the 3D geometry of the stents *in-situ* (RhinoCAD software, McNeel, WA, USA; Schievano et al., 2010b) at the end of balloon inflation, and at early systole and diastole (Fig. 2). From these reconstructions, the displacements of every strut junction of the stent from the end of balloon inflation through systole and diastole were calculated. Circumferential, radial and longitudinal asymmetries were measured for each time step and every patient. The stent expanded into the patients' implantation sites resembled the outline of their arterial walls, resulting in asymmetry in all directions (Fig. 3top). In particular, some of the stent struts were at an early stage of expansion, while others were over-deployed compared to a uniformly deployed stent in a cylinder. The most expanded cells were located in correspondence to the fracture positions as detected from x-rays images in the patients. Furthermore, in all studied patients, the stents were non-circular in cross-section and the terminal rings were more expanded if compared to the central portions.

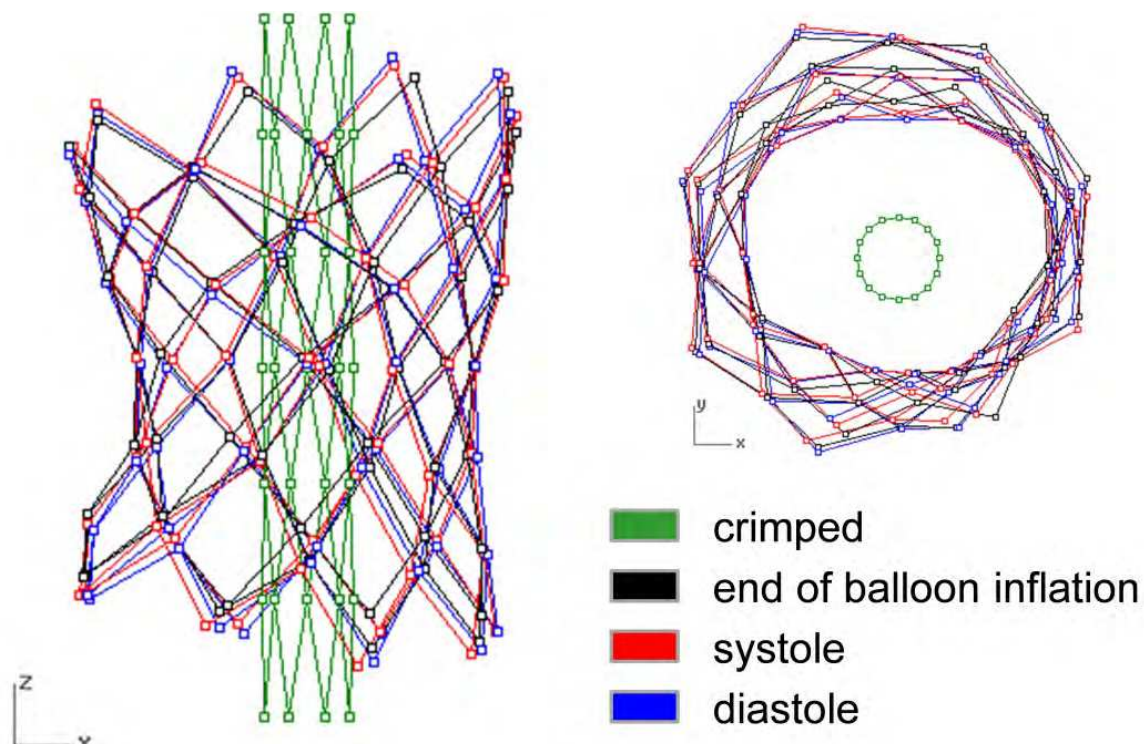


Fig. 2. Superimposition of the stent fluoroscopy reconstructions for one patient at the end of balloon inflation, systole, and diastole compared to the initial crimped configuration (lateral and top views)

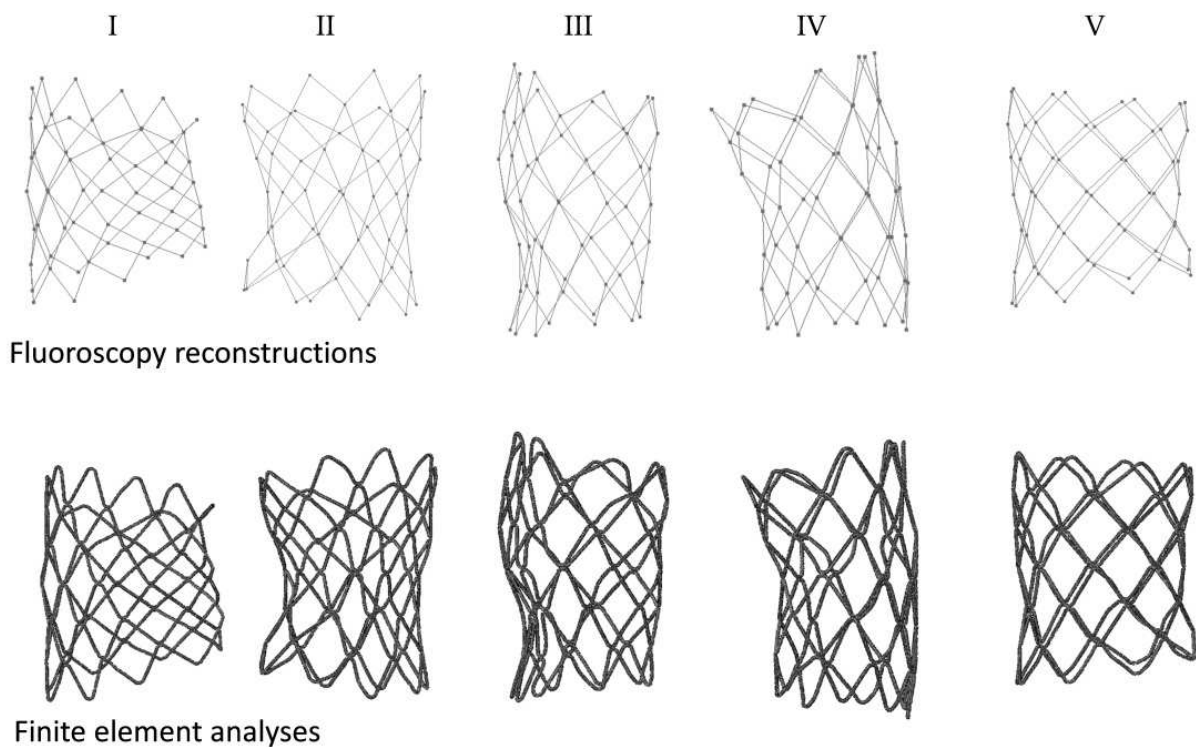


Fig. 3. Stent fluoroscopy reconstructions for the analysed patients at diastole (top panel) and corresponding FE deployed configurations (bottom panel)

A FE model of the crimped stent in the catheter was created, with a structured hexahedral mesh of 119,360 elements to model the platinum-iridium wires. To reproduce the golden coverings, an additional set of elements was modelled around the junctions and a structured hexahedral mesh was generated using 36,320 elements. Stent geometrical and material properties were provided by the manufacturer (Table 1; Schievano et al., 2007c).

PPVI stent

<i>Geometry</i>	
Wire diameter	0.33 mm
Crimped configuration internal diameter	4.00 mm
Crimped configuration overall length	34.32 mm
Central zig-zag segment length	5.78 mm
Terminal zig-zag segment length	5.62 mm
<i>Platinum-10% Iridium</i>	
Young modulus	224 GPa
Poisson ratio	0.37
Yield stress	285 MPa
Ultimate strength	875 MPa
Fatigue endurance strength	263 MPa
<i>Gold</i>	
Young modulus	80 GPa
Poisson ratio	0.42

Table 1. Stent geometrical and material properties

Patient-specific stent deployments were replicated in Abaqus/Standard (Simulia, RI, USA) using nodal displacement boundary conditions (Fig. 3bottom). These displacements were those previously calculated from fluoroscopy reconstructions and were applied to the central node of each stent strut junction. Three displacement steps were performed to account for the full loading history of the stent and potential residual stresses: the first step resulted in the stent deployment from its initial crimped status to the end of balloon inflation; the second and the third steps replicated a cardiac cycle from systole to diastole. The elements surrounding the nodes of displacement application were subtracted from the model in the analysis of stress outcomes because they resulted distorted due to the type of displacement condition adopted. This was considered acceptable as fractures at the strut junctions have not been reported for the current stent after golden reinforcements were introduced.

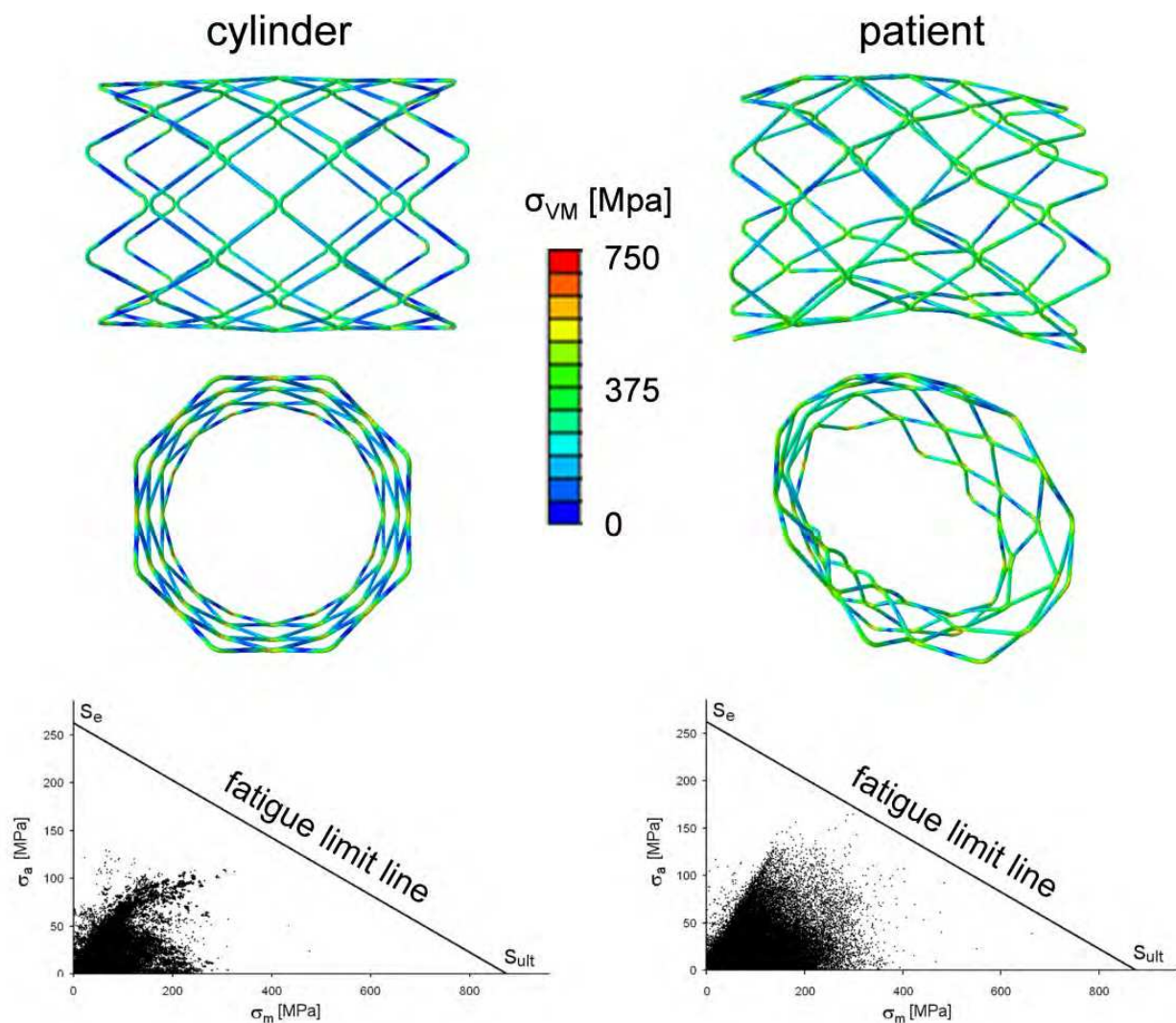


Fig. 4. Comparison of the stress distribution and Goodman diagrams between the stent deployed in a cylindrical configuration, as performed during conventional preclinical testing, and the stent deployed according to individual *in-situ* geometry from 1 of the studied patients. Goodman diagrams are a graphical representation of fatigue analysis (σ_m and σ_a = mean and alternating stresses, while S_{ult} and S_e = material ultimate and fatigue endurance strengths)

Stresses in the stents after deployment in patients' configurations were higher if compared to the same stent uniformly expanded in a cylindrical geometry as done during conventional preclinical testing, and, therefore, the risk of reaching the endurance limit of the material was higher (Fig. 4). The highest stresses occurred close to the strut junctions, which were the most highly bent portions of the device. The peak σ_{VM} was reached during diastole in every patient, and its values ranged between 516.1 and 612.8 MPa.

A fatigue analysis was performed by applying the Goodman method (Beden et al., 2009; Marrey et al., 2006) and the Sines criterion (Sines & Ohgi, 1981). The first uses a graphical approach to relate alternating stress (σ_a) and mean stress (σ_m) during the cardiac cycle with the material strength limits (Fig. 4), where σ_a and σ_m are calculated as follows:

$$\sigma_m = \frac{\sigma_{sys} + \sigma_{dia}}{2} \quad \text{and} \quad \sigma_a = \frac{|\sigma_{sys} - \sigma_{dia}|}{2}$$

with σ_{sys} and σ_{dia} equal to the maximum principal stresses at the end of the systolic and diastolic phases respectively.

The second is a multi-axial fatigue criterion that uses the equivalent Von Mises stress as control parameter. To evaluate the fatigue resistance with the Sines criterion, the equivalent Sines stress, for the comparison with the material fatigue endurance strength S_e , was calculated as in the first member of the following disequation: $\sqrt{3}(\sqrt{J_2})_a + 3\frac{S_e}{S_{ult}}\sigma_{H,m} \leq S_e$

where $(\sqrt{J_2})_a$ and $\sigma_{H,m}$ are the amplitude of the mean square root of the second deviatoric stress invariant and the hydrostation pressure, respectively.

During the cyclic loading condition, the stent in the patients worked at high σ_m and σ_a , if compared to a uniformly deployed stent, thus indicating a high number of areas at risk of fatigue failure as shown by the Goodman distributions (Fig. 4). The portions at highest potential for fracture were non-uniformly distributed amongst the different studied cases, with highest values in the areas close to the strut junctions, where indeed such fractures

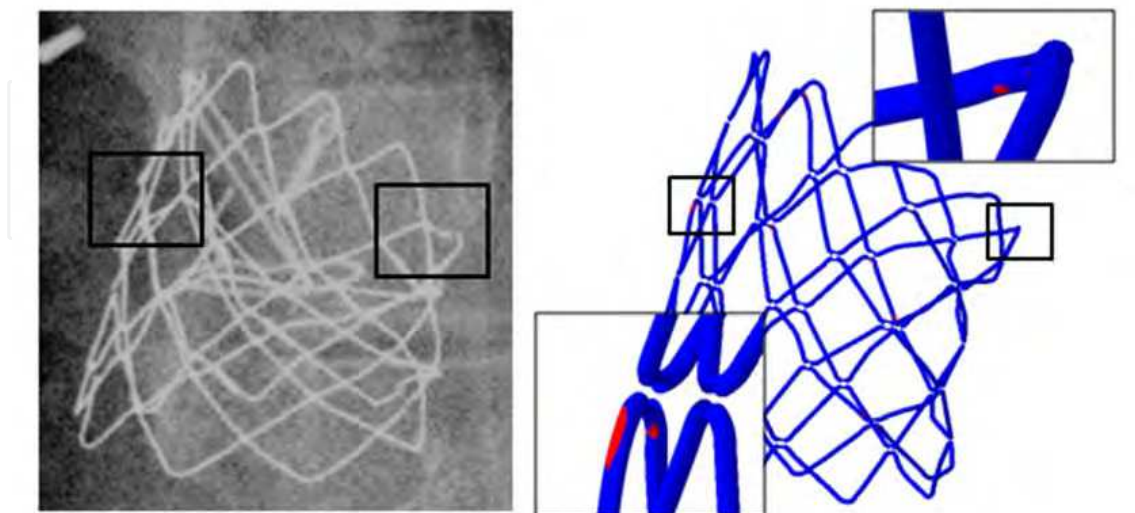


Fig. 5. X-ray image of the stent *in-vivo* in 1 of the analysed patients at 3 months follow-up compared to the Sines stress map in the corresponding patient FE simulation with areas at highest risk for fracture highlighted in red

occurred in the patients (Fig. 5). The Sines criterion predicted fractures in every case, with the most stressed regions in 3 cases close to the strut intersections between the first and the second ring from the proximal end; in one case it was at the lowest terminal crown and in the last patient it was detected between the second and the third crown.

Reproducing patient-specific FE analysis with more realistic loading conditions can provide more accurate information regarding the stent mechanical performance and prediction of fatigue life compared to the conventional bench methodologies/FE analyses/ of free/cylindrically constrained expansion. Indeed, this computational analysis predicted failure and the locations of fractures were similar to the sites where the patients ultimately had stent damage.

2.1.2 Stent-in-stent as a potential solution to stent fractures

FE analysis can also give insight into improved clinical management. This is demonstrated by a FE analysis of stent mechanical performance for various combinations of stent designs. Inserting a separate stent into the pulmonary artery prior to the PPVI device (stent-in-stent technique, Nordmeyer et al., 2008) may reduce valved stent fractures. An optimised combination of different stent mechanical properties can help increase the strength of the device structure while at the same time reduce the stresses. This was computationally tested by expanding 2 PPVI stents 1 inside the other (Schievano et al., 2007c). The mechanical performance of the coupled device was compared with that of a single valved stent, expanded and cyclic loaded at the same conditions. The stresses in the outer stent of the coupled device were similar to those of the single valved stent. However, the stresses in the coupled device inner stent, which holds the valve, were lower when compared to the stresses in the single valved stent (Fig. 6), thus decreasing the risk of fracture for the valved stent.

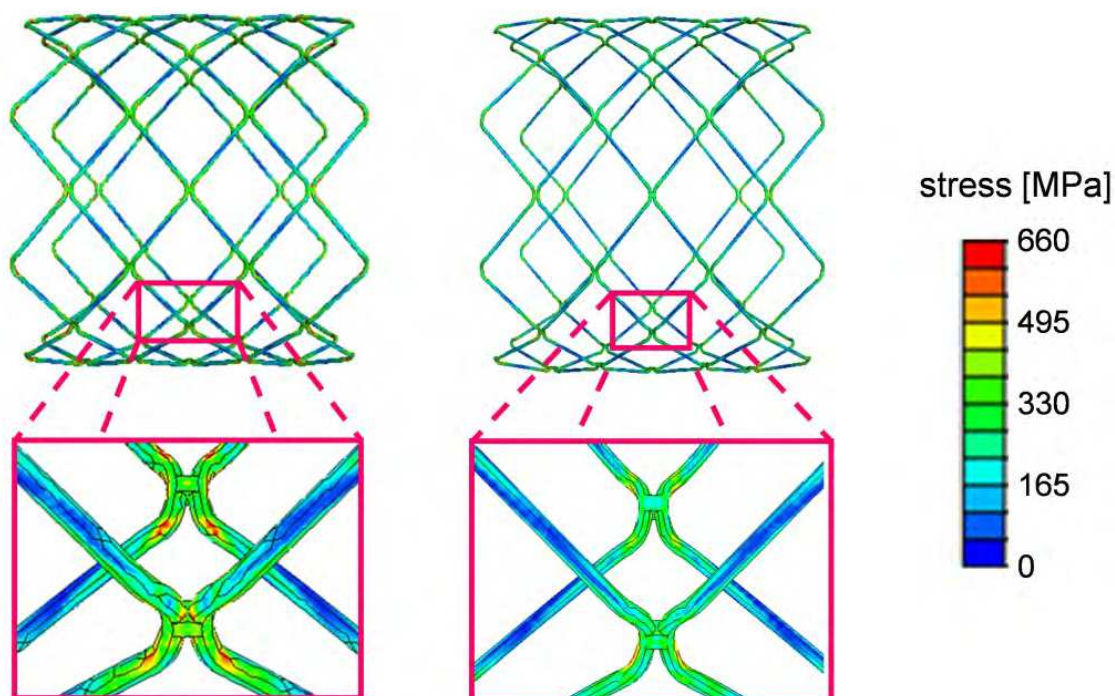


Fig. 6. Stress distributions in the single valved stent and in the inner valved stent when 2 devices are coupled together (stent-in-stent)

The implantation of a previous device before the valved one acts functionally to bolster the vessel and reduce the stresses on the stent. This information, in combination with the computational modelling described above, suggests that pre-stenting may ensure the integrity of the valved device, thus enhancing the success of the percutaneous procedure. Indeed this is the case when we look at patients who undergo pre-stenting, where the risk of developing a stent fracture is reduced (Nordmeyer et al., 2011). However, this solution is still limited to those patients with suitable implantation sites and the current device does not fit all the sizes of patients requiring pulmonary valve treatment. New devices have to be developed to offer this minimally invasive procedure to the entire patient population.

2.2 Next generation device

Despite the success of the PPVI device, <15% of patients requiring pulmonary valve replacement can be treated with the current PPVI device, with the remaining 85% requiring open-heart surgery (Schievano et al., 2007a). The majority of these patients are those with dilated, dynamic pulmonary arteries in whom the current percutaneous device is too small. Importantly, for this morphological problem, animal testing is of very limited use, as there are no models that encompass the wide variations of anatomy seen in these patients with congenital heart disease. Hence development of a new device to deal with the clinical problem and its translation into man is difficult using the conventional pathway of bench followed by animal testing.

Over the last 5 years, a new PPVI device for implantation into the dilated pulmonary artery has been developed in collaboration with Medtronic Cardiovascular. The device is made from self-expandable nitinol zig-zag rings, held together by a polyester graft in an hourglass shape (Fig. 7). The extremities of the stent, with larger diameters, would ensure the anchoring of the device against the pulmonary artery, while the central rings, with smaller diameter, would act as supporting structures for the valve. Nitinol is a shape memory alloy regularly used in bioengineering applications because it combines important qualities such

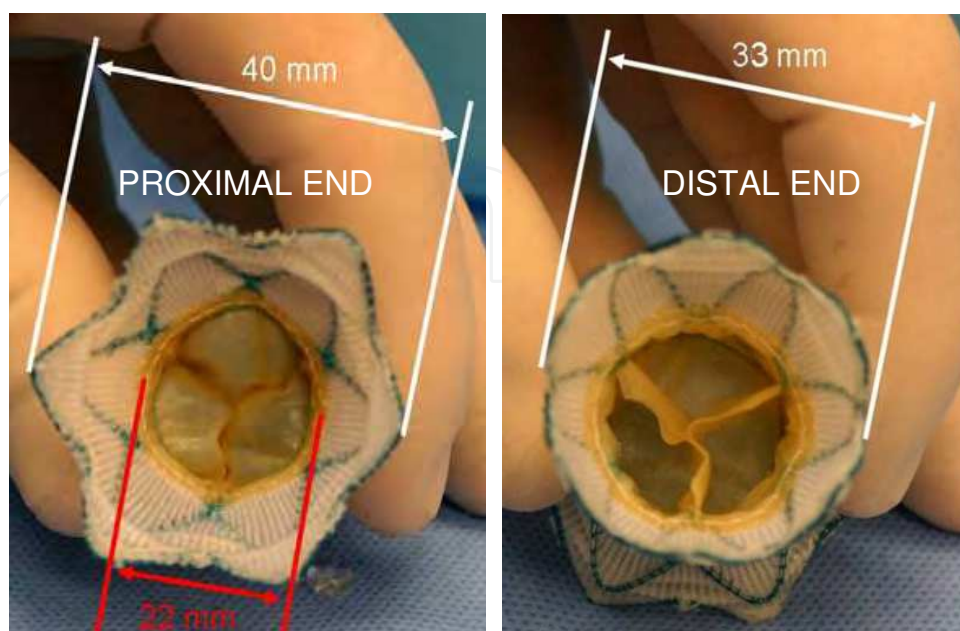


Fig. 7. New PPVI device and dimensions

as biocompatibility, fatigue resistance, and magnetic resonance (MR) compatibility, with the peculiar mechanical behaviour to undergo large completely recoverable deformations (Petrini et al., 2005). The valve is made of porcine pericardium and is sutured in the central portion of the stent-graft. Conventional animal testing and bench testing had been undertaken for this device and demonstrated a good performance in the animal model (Bonhoeffer et al., 2008). This stent-graft design should guarantee a greater adaptability of the device to the wide range of possible implantation site morphologies, with long-term fatigue behaviour that dramatically outperforms conventional metals.

2.2.1 First-in-man application

During the final stages of the preclinical testing of the new device, a patient presented to our Institution requiring pulmonary valve replacement (Schievano et al., 2010a). This patient (42-year-old man with congenital heart disease) had previously undergone 4 open-heart operations and 2 additional thoracic procedures, and remained highly symptomatic with severe pulmonary insufficiency. A further cardiothoracic surgery was considered too high risk. In addition, the pulmonary artery was too dilated for the current PPVI device. Therefore, the patient was considered for implantation of the new device. An integrated strategy to pre-clinical testing, using patient imaging data, computer modelling and biomedical engineering was developed to influence the final device design for implantation.

4D cardiovascular computed tomography (CT) was performed to acquire 3D volumes of the implantation site over 10 frames of the cardiac cycle (CT-SOMATOM Definition, Siemens Medical Systems) according to previously described methodologies (Schievano et al., 2007a), and to measure the 3D deformations in terms of diameter changes at different sections (Fig. 8a; Schievano et al., 2011). Based on the CT implantation site reconstructions (Mimics, Materialise, Belgium), FE models (Fig. 8b) and 3D rapid prototyping (Fig. 8c) models were created (Schievano et al., 2007b; Schievano et al., 2010b). Multiple device shapes and sizes with varying wire stiffness and configurations were tested in the rapid prototyping models and using FE analysis to optimise the anatomical results in the specific patient: the FE analysis identified definitive areas of contact between the computer simulated stent-graft struts of the customized device and implantation site, predicting likely stability and safe anchoring in-vivo. The rapid prototyping models enabled simulation of the clinical implantation procedure and helped the implanters decide the approach for optimal device delivery.

The final device (40 mm diameter in the distal and proximal ring, 22 mm diameter in the central portion holding the valve) underwent acute and chronic animal tests and bench testing. Based on these results, the UK Medicines and Healthcare products Regulatory Agency (MHRA), and the local ethical and industrial committees granted approval for the use of this device on humanitarian grounds. The patient gave informed consent for the procedure and for the anonymous use of his data and images for research.

PPVI was successfully carried out in this patient with the new device in January 2009. During the catheterisation procedure, angiographic studies and balloon sizing of the pulmonary trunk were performed and confirmed that the CT and model dimensions were a true representation of the patient's anatomy. The delivery strategy developed from the pre-procedural trial implantation in the rapid prototyping models was followed and proved safe

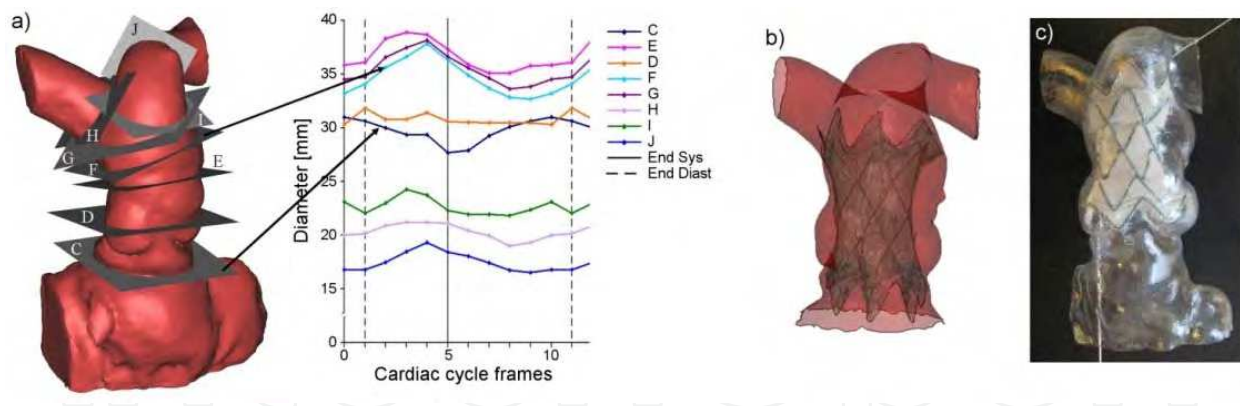


Fig. 8. a) 3D volume reconstruction of the patient's implantation site from 4D CT and diameter change measurements over the cardiac cycle measured in the 8 selected planes (C-L). Examples of b) FE model, and c) plastic rapid prototyping model (guidewire in place) of the patient anatomy with the new PPVI device "implanted" to test different positions, anchoring, and delivery approaches

and successful (Fig. 9a). The patient was symptomatically improved following the procedure. A post-implantation 4D CT confirmed that the device had the position, shape and safe anchoring as predicted by the FE models (Fig. 9b). These post implantation CT images were used to reconstruct the stent geometry *in-situ* and to assess the 3D displacements of the device rings over the cardiac cycle. This information was inputted in a FE analysis as explained above to predict the likelihood of stent fracture. The patient remains well 3 years following the procedure, with no fractures of the stent struts detected to date, as predicted by the FE study.

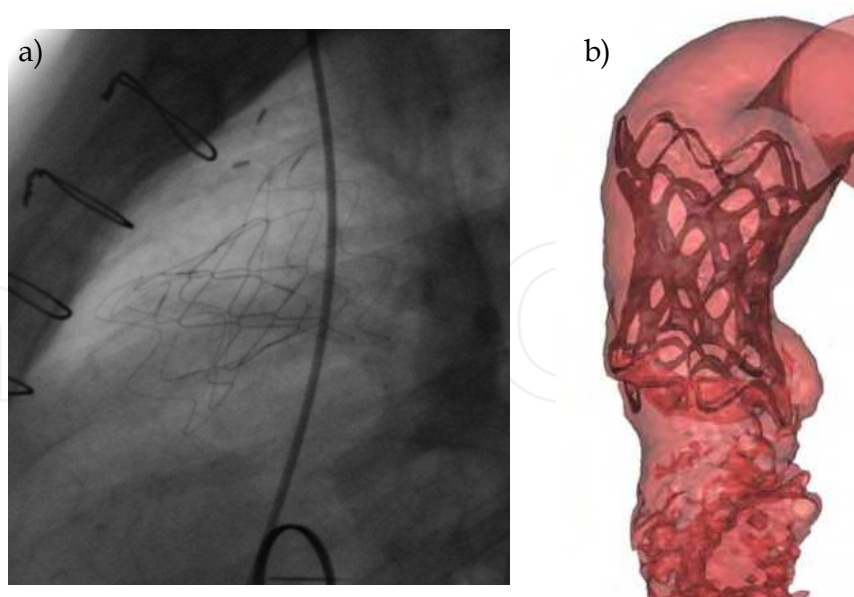


Fig. 9. Lateral view of a) x-ray fluoroscopy, and b) 3D volume CT reconstruction of the new PPVI device, 2 days after implantation in the patient

Whilst such a labour intensive method, which resulted in modifications in the device design prior to this first human case, was essential to enable us to safely transfer this new

technology into early clinical practice, this approach would not be necessary, or sustainable, for each patient in routine clinical practice. Ultimately, the aim for this new PPVI technology would be to have a small number of 'off-the-shelf' devices with varying sizes and shapes, which would be suitable for the vast majority of patients. In order to optimise the number of devices necessary to cover the whole range of patients' morphologies, we used FE analysis taking into account patient specific anatomies (Capelli et al, 2010a).

2.2.2 Optimisation of the next generation device

FE modelling is a powerful tool to optimise device design without the need for many prototypes to be created and tested. In pulmonary valve dysfunction, each patient anatomy is completely individual in terms of size, shape and dynamics. FE can help select the most appropriate prosthesis for any individual patient taking into account their specific anatomy, thus enhancing the safety and success of the procedure. Furthermore, FE analysis can help predict how many devices may be needed to cover the whole range of patient morphologies.

Three different potential designs for the new stent-graft were considered, with equivalent central ring diameters (22 mm), but different proximal and distal strut dimensions (Fig. 10; Capelli et al, 2010a): the first stent-graft (SG1) resembled the device that had already been successfully tested in animals (Bonhoeffer et al, 2008). The second stent-graft (SG2) was symmetrical, similar to the device implanted into the patient described in the previous paragraph (Schievano et al, 2010a). The third stent-graft (SG3) was similar to SG2, but with larger proximal and distal diameters. 1D beam elements were chosen to mesh the stent wires (696, 696 and 912 elements for SG1, SG2 and SG3, respectively). Surfaces were created in between the struts to model the polyester fabric, which was meshed using membrane elements that offer strength in the plane of the element, but have no bending stiffness (3850, 3408 and 3909 elements for SG1, SG2 and SG3, respectively). A tight, rigid contact was assumed to simulate the suture between the stent and the graft. The shape memory alloy model implemented in Abaqus code was used to describe the nitinol behaviour of the stent wires. A hyperelastic, isotropic constitutive model based on a reduced polynomial strain

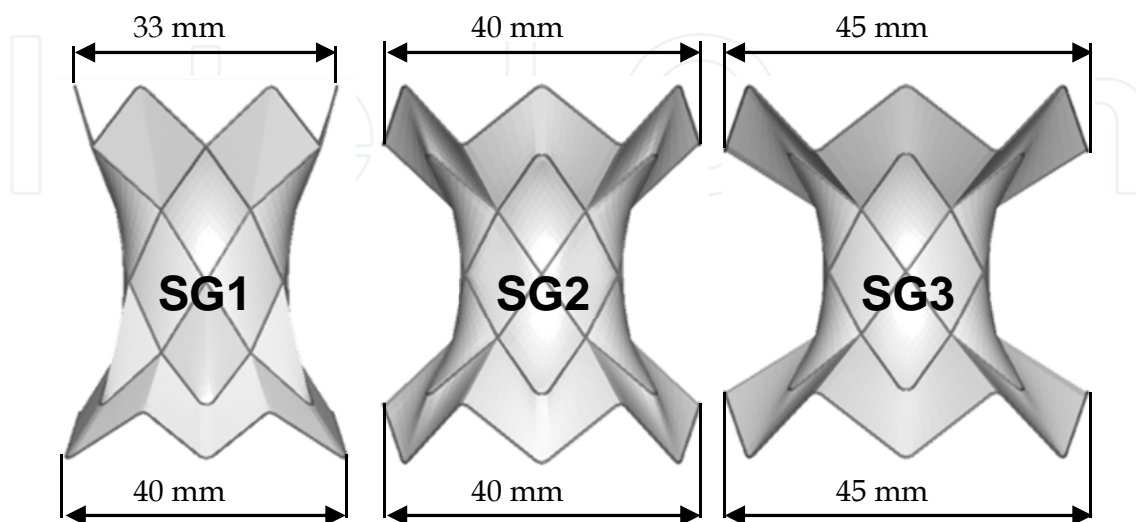


Fig. 10. Models of the 3 stent-grafts SG1, SG2 and SG3 designed and tested using FE analysis

energy density function ($C_{10} = 0.38$, $C_{20} = 4.36$, $C_{30} = 80.56$, $C_{40} = -134.72$, $C_{50} = 86.24$, $C_{60} = -19.74$) was used for the fabric graft material. The material FE models were validated using experimental tensile tests carried out for the nitinol wires and fabric samples. The valve was neglected in the FE analyses.

Pre-operative 3D MR data (1.5 T Avanto, Siemens Medical Systems) from 62 patients who were morphologically or dimensionally unsuitable for the current Melody™ device were used to reconstruct rigid FE models of the implantation sites – rigid 3D shell elements with number of elements varying between 7,172 and 13,104 according to the complexity of the patient implantation site geometry (Capelli et al, 2010a).

The 3 stent-grafts' FE models were placed inside each patient's outflow tract model, as close as possible to the bifurcation, without obstructing the pulmonary arteries. The implantation of the devices was carried out by crimping the stent-grafts down to 7 mm diameter (catheter dimensions) and then releasing them inside the patients' outflow tract models (Abaqus/Explicit). A general contact algorithm was defined to allow interaction between the devices and the arterial wall. The stent-grafts adapted their shape to the implantation site of each specific patient (Fig. 11). The diameters after deployment were quantified in the proximal, central and distal sections of the stents to judge the safe anchoring of the device inside the artery, which was considered optimal if the proximal and distal diameters measured less than 80% of the original diameters, according to manufacturer's specifications. Furthermore, the central portion of the device should be >18 mm so that the valve sewn inside can be fully deployed.

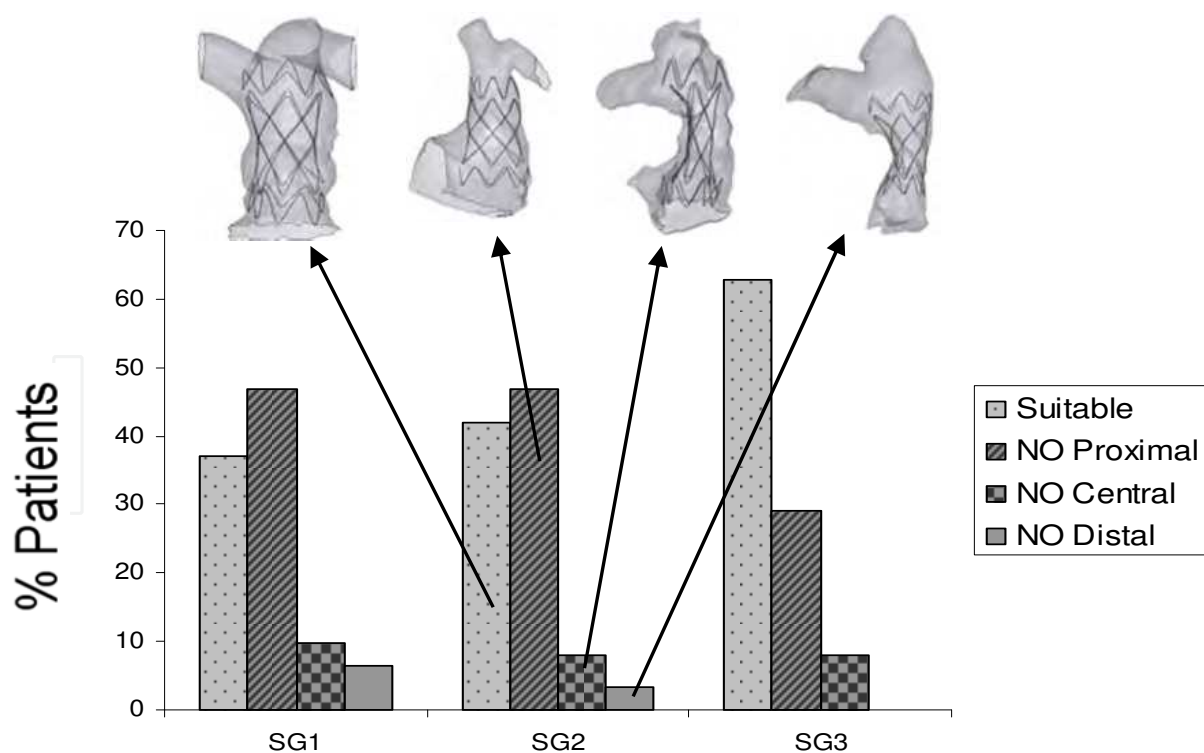


Fig. 11. Percentage of suitable and not suitable patients for SG1, SG2, and SG3 and examples of patients in which device SG2 was virtually implanted. Unsuitable patients are subdivided according to the regions of the stent that did not respect the criteria of safe implantation

According to these criteria, successful implantation was achieved in 37% of the patients with SG1. 42% of the patients would be suitable for the SG2 device and 63% for the SG3 device (Fig. 11). Therefore, 37% of those patients who are currently still treated with surgery would potentially be suitable for PPVI with a new device. Furthermore, if the dimensions of this new device are theoretically increased at the distal end (SG2, as done for the first-in-man case) or both proximal and distal ends (SG3), the number of percutaneous procedures would increase by a further 5% and 36%, respectively. Importantly, these dimensions would be difficult to test in animals because of lack of relevant sizes in these settings. Although animal testing remains important, FE modelling could be integrated into preclinical testing to predict how such devices behave when implanted into the human situation.

With the introduction in clinical practice of the new device in 3 sizes, the total number of patients requiring pulmonary valve replacement who could benefit from a percutaneous approach (current device + 3 sizes of the new device) would be approximately 70%. This would potentially have a big impact on the cost benefit for healthcare, by reducing hospital stay and improving the speed at which patients can get back to normal daily activities.

3. Transcatheter aortic valve implantation

In the past decade, TAVI has been shown to be a feasible and effective option for treatment of patients with symptomatic severe aortic stenosis and high operative risks (Leon et al., 2011; Rodes-Cabau et al., 2010; Smith et al., 2011; Vahanian et al., 2008; Zajarias & Cribier, 2009). Since the first-in-man experience in 2002 (Cribier et al., 2002), several advances in TAVI techniques have led to improved success rates, with acceptable procedure-related complication rates (Delgado et al., 2010). To date, 2 different devices have received CE mark approval - the balloon-expandable Edwards-Sapien® XT Valve (Edwards Lifesciences, CA, USA) and the self-expandable CoreValveReValving System® (Medtronic) - with many other devices emerging into the market (Fig. 12). The encouraging mid- and long-term results of



Fig. 12. TAVI Edwards-Sapien® Valve and the self-expandable Medtronic CoreValve ReValving System® (http://mail.c2i2.org/web10-06/transcatheter_aortic_valve_implantation.asp)

this technique, together with increased patient comfort, shortened intensive care and hospital stay, and the avoidance of cardiopulmonary bypass, make this non-surgical technique extremely appealing (Ussia et al., 2009).

Accurate multidisciplinary pre-procedural evaluation of patients who are considered candidates for TAVI is mandatory to plan the most adequate treatment and to minimise peri- and post-procedural complications (Smith et al., 2011; Vahanian et al., 2008). However, in this emerging field, several issues remain a source of debate. Device sizing and positioning are the main challenges, but vascular complications, electrical conduction abnormalities and post-procedural aortic regurgitation still remain major safety concerns. In addition, according to the current position statement, TAVI is indicated only in patients with severe symptomatic aortic stenosis, and who are considered at high or prohibitive risk for conventional surgery (Ussia et al., 2009, Leon et al., 2011).

Extending TAVI to patients who still undergo conventional surgery poses new challenges, both for clinicians and device manufacturers, but “within 10 years, with further improvement of the devices and procedures, and depending on the long-term results of upcoming controlled trials in a broad population, TAVI may become the treatment of choice in a majority of patients with degenerative aortic stenosis” (Cribier, 2009). Indeed, highly experienced centres have already demonstrated the feasibility of TAVI in failed bioprosthetic heart valves (valve-in-valve procedure) in patients considered at very high-risk or ineligible for surgery (Webb et al., 2010). Previous surgical valve implantations represent a well-defined landmark with rigid boundaries that increase ease of positioning and anchoring, thus making patients with bioprosthetic valves ideal candidates for TAVI (Walther et al., 2011). Conversely, younger patients, with less severe aortic valve stenosis or with valve insufficiency, often present implantation sites with different anatomical and dynamic characteristics that generate procedural and device related hurdles, which means that such patients are currently not suitable for or offered TAVI.

Combining patient-specific imaging data and computational modelling offers a new method to obtain additional, predictive information about responses to cardiovascular device implantation in individual patients (Schoenhagen et al., 2011; Taylor & Figueroa, 2009). FE analyses were performed to explore the feasibility of TAVI using a model of the Edwards-Sapien® device in specific patient morphologies which are currently borderline cases for a percutaneous approach. This method can help in both refining patient selection and characterising device mechanical performance, overall impacting on procedural safety and success in the early introduction of TAVI devices in new patient populations.

3.1 Patients with previously implanted bioprosthetic valves

Four patients with different stenotic bioprosthetic valves previously implanted (patients A – 23 mm Carpentier-Edwards Perimount Magna valve, Edwards Lifesciences; B – 23 mm Soprano™ valve, Sorin Biomedica Cardio, Italy; C – 25 mm Carpentier-Edwards Perimount valve, Edwards Lifesciences; D – 25 mm Epic™ valve, St Jude Medical, MN, USA) and who were referred for surgical replacement of their failing bioprosthetic valve were analysed (Bosi et al., 2010; Migliavacca et al., 2011). Data about the anatomy of the aortic root, coronary arteries, AV leaflets and bioprostheses were acquired using CT imaging (CT-SOMATOM Definition) and these data were used to reconstruct 3D geometries for FE

models of the selected patients' implantation sites (Fig. 13). The aortic roots were assumed to be 2 mm thick, with density equal to $1,120 \text{ kg/m}^3$ (Conti et al., 2010) for all models and meshed with 3D triangular shell general-purpose elements (Table 2). To describe the mechanical behaviour of the aortic roots, Mooney-Rivlin hyperelastic behaviour was adopted incorporating experimental stress-strain data for the ascending aorta (Okamoto et al., 2002) and taking into account the pre-stretching of the aortic root due to the aortic pressure during the cardiac cycle.

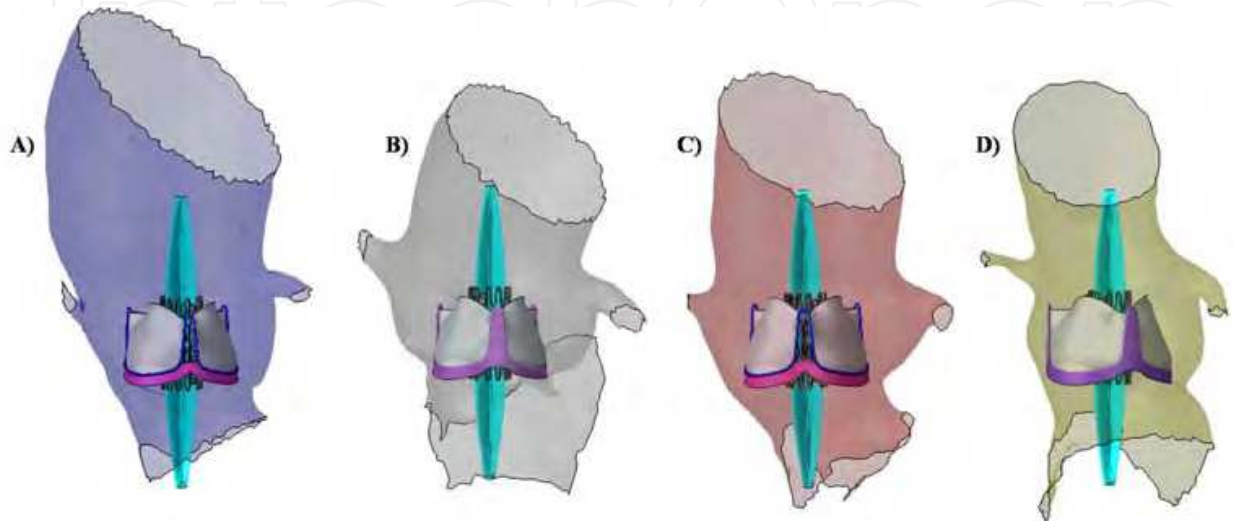


Fig. 13. CT image reconstruction of the selected patients' aortic wall with previously implanted bioprosthetic valves. FE models of the deployment balloon and TAVI stent are placed inside the implantation site models

Part	Elements
<i>Patient-specific model</i>	
A	6,875
B	8,675
C	11,325
D	8,347
<i>Bioprosthesis (stent + leaflets)</i>	
Perimount Magna	44,048 + 29,021
Soprano	51,372 + 28,667
Perimount	44,048 + 29,021
Epic	51,372 + 28,667
<i>TAVI device</i>	
Sapient stent	192,920
Balloon	8,160

Table 2. Number of mesh elements for the different parts involved in the FE simulations

The metal frames of the 4 bioprosthetic valves were reconstructed from the CT images to identify their position inside the patients' outflow tracts. The bioprosthetic valve geometries were re-drawn using CAD software (Rhinoceros) to recreate a complete model of the corresponding commercial device used in the patients, and then placed in the same position as that identified from CT images. Connector elements were used to link the bioprosthetic

valves with the aortic vessels to mimic the suture between the ring and the aortic root. Each prosthesis included different frame structures, sewing rings and artificial valve leaflets. The frames (metallic and polymeric) were meshed with 8-node linear hexahedral elements with reduced integration (Table 2), and modelled using an elasto-plastic constitutive behaviour obtained from the manufacturer's data. Bovine and porcine valve leaflets were meshed with 4-node, quadrilateral, shell elements with reduced integration and large-strain formulation (Table 2), while the material properties were simplified using a linear, elastic model (Lee et al., 1984; Zioupos et al., 1994). Calcification of the leaflets was created by increasing Young's modulus and thickness in the region of the commissures (Loree et al., 1994), where a weld constraint was also applied (Schievano et al., 2009): 16 connector elements per commissure were added. An axial, rigid behaviour was assigned to the connectors, allowing them to maintain a fixed distance between the 2 nodes until a threshold force was reached – equal to 0.92 N (Loree et al., 1994) along the direction joining the 2 nodes – and then fail after this threshold value was reached, mimicking calcification failure. The thickening and welding of the failing valve leaflets produced aortic valve geometric orifice areas equal to those measured in the selected patients (1.2 cm² for A and B, and 1.4 cm² for C and D).

The Edwards-Sapien® stent is characterised by 12 units, each formed by 4 zigzag elements (Fig. 12). A vertical bar divides each unit and a perforated bar is positioned every 4 units. The CAD geometry of this stent was reproduced with a height, internal diameter and thickness of the expanded stent equal to 16.0, 25.4 and 0.3 mm, respectively. The stent was meshed with hexahedral elements, following mesh sensitivity analysis. It is made of stainless steel which was modelled using Von Mises plasticity behaviour from manufacturer data.

A semi-compliant balloon was designed to resemble the commercial balloon used in clinical practice (Z MED II™, NuMed Inc, NY, USA) and placed inside the TAVI stent in order to deploy the device (Capelli et al, 2010b; Gervaso et al., 2008). The balloon was meshed with 0.03 mm thick membrane elements, and a homogeneous, isotropic, linear-elastic Nylon11 was adopted according to manufacturer data. The stent was crimped down onto the balloon, from its original configuration to catheter dimension (8 mm diameter), using a coaxial cylindrical surface.

The stent-balloon system was placed into the aortic root models according to the judgment of 2 clinicians (Fig. 13). Large deformation analysis of stent deployment in the patients' implantation sites, performed with Abaqus/Explicit, was divided in 2 different steps: balloon pressurisation with resulting stent expansion in the aortic root, and balloon deflation with subsequent stent recoil. In all patients, the implantation site model extremities (upper and lower aortic sections and coronary terminal sections) were constrained in all directions (circumferential, radial and longitudinal) in order to mimic the connection with biological structures. Boundary conditions on the balloon were placed to mimic the bond with the catheter.

Contact properties were defined to describe the interactions encountered in these multi-part analyses. Interactions included contact between surfaces belonging to balloon and TAVI stent, balloon and bioprosthetic aortic valve leaflets, TAVI stent and bioprosthetic aortic valve, bioprosthetic aortic valve and aortic wall. Friction between Nylon and stainless steel was included in the model with coefficient equal to 0.25 (De Beule et al., 2008).

Mechanical performance of the stent and the impact of the TAVI device into patients' implantation sites were evaluated by analysing: stent configurations at the end of balloon inflation, stent recoil after balloon deflation, stent and arterial stress distribution and peak values at the end of the expansion and recoil phases, degree of aortic valve stenosis assessed according to the post-TAVI geometrical orifice area, and evaluation of coronary artery obstruction.

At the end of all simulations, the TAVI stent was virtually implanted inside the bioprostheses of the patient-specific aortic root model, with a position that was found in good agreement with available images from a TAVI follow-up case (Fig. 14, Webb et al., 2010).

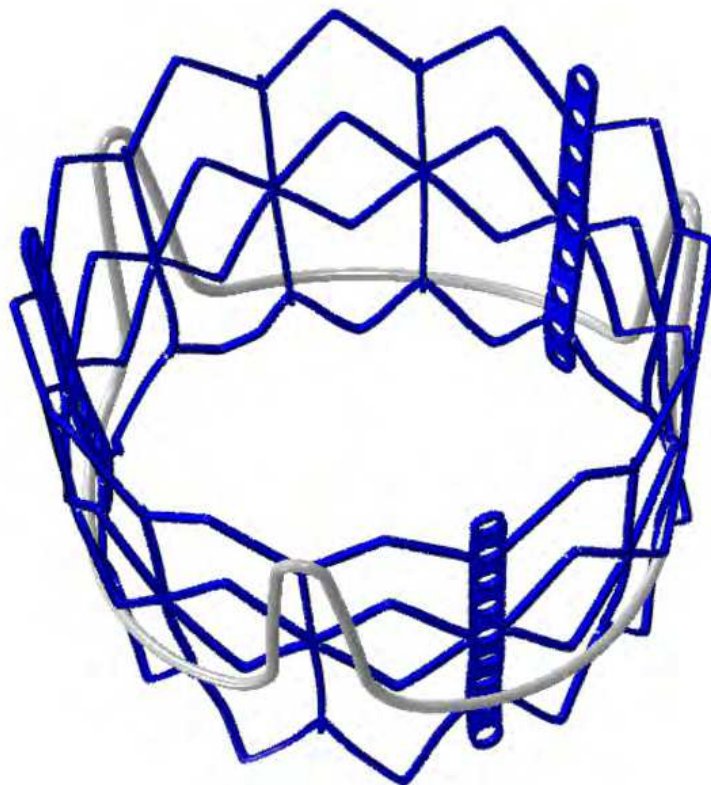


Fig. 14. Result from the FE simulation of TAVI stent in a Carpentier-Edwards bioprosthesis, resembling the CT image reconstruction of a patient's TAVI in the same bioprosthetic valve published by Webb et al., 2010

After deployment, the stent assumed an asymmetrical configuration in the longitudinal direction, more expanded in the distal part. There was no contact with the native aortic wall and/or other cardiac structure. This was also demonstrated by the low stresses (<0.1 MPa) measured in the aortic wall, showing how the previously implanted bioprostheses act as a scaffold for the TAVI stent. After balloon deflation, the bioprosthetic valve leaflets partially recoiled forcing the TAVI stent to a more symmetrical shape, which could be defined almost cylindrical in all cases (Fig. 15). Maximum recoil was measured in the distal sections for all patients (A = 17.0%; B = 13.2%; C = 11.7%; D = 10.8%) with absent or low recoil at the level of the bioprosthetic valves' annulus.

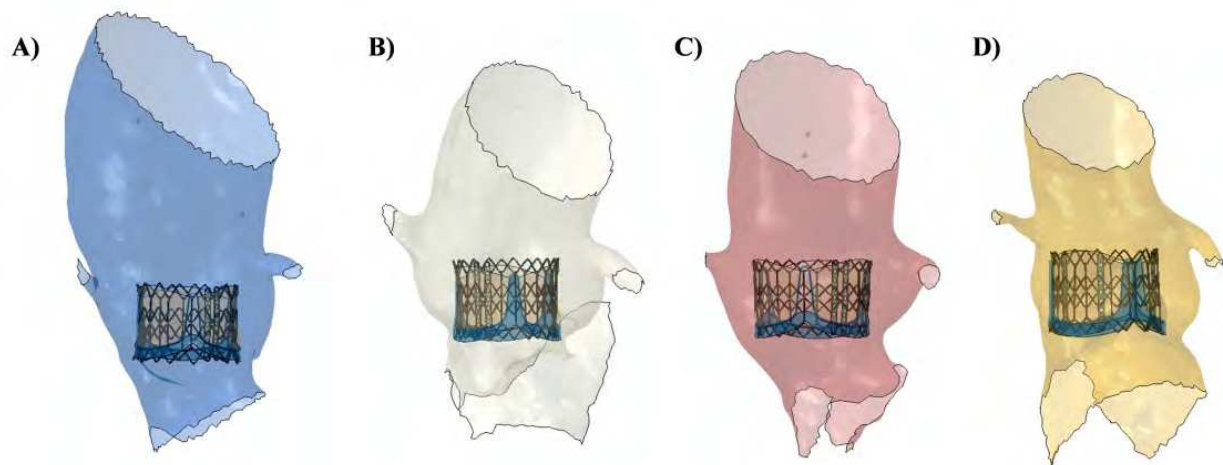


Fig. 15. TAVI stent final configuration (end of balloon deflation) in the patients' models

At the end of both the expansion and recoil phases, for all models, non-uniform stress distribution was recorded on the stent struts with the highest Von Mises stresses occurring at the strut junctions with the vertical bars (Fig. 16). At the same locations material plasticisation was reached that guaranteed final open configurations. If we compare the results from the patient-specific simulations with those of a stent uniformly deployed in a cylinder, which is the idealised implantation site used in conventional preclinical testing of

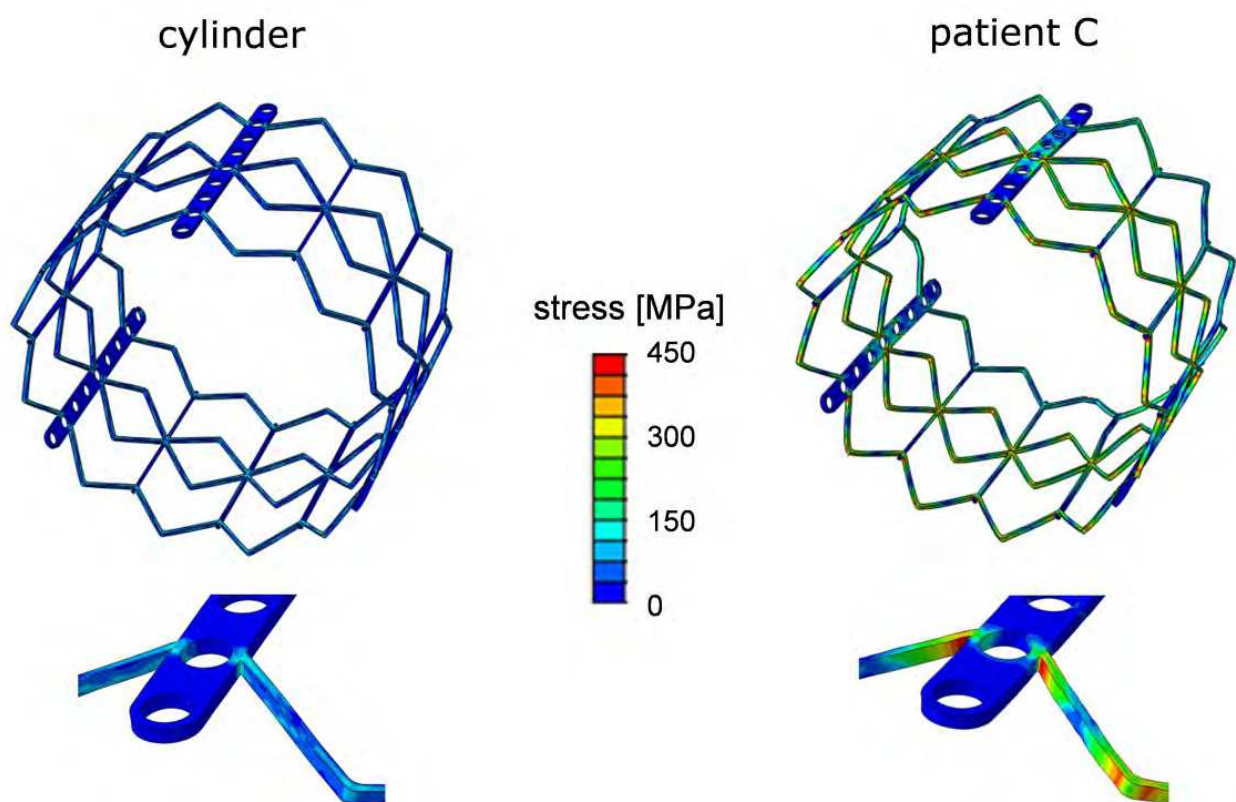


Fig. 16. Von Mises stress distribution in the TAVI stent after balloon deployment and deflation in a cylindrical configuration and in patient C

such devices, the maximum stress reached in the stent deployed in the patients was significantly higher than the stress in the stent deployed in the cylinder (443 vs 270 MPa). In addition, the stent was uniformly deployed in the cylinder during the entire simulation: recoil between the steps of balloon inflation and deflation was low (1.5%) and uniform along the stent length. The non-uniform shape of the deployed configuration in the patients and, therefore, the asymmetric stress distribution might cause long-term stent failure due to the pulsatile loading conditions during the cardiac cycle that are not seen during conventional pre-clinical tests (Schievano et al., 2010b).

After simulated TAVI, the connectors modelling calcification of the leaflet commissures were all broken, thus increasing the aortic valve geometrical orifice area to 3.43, 3.60, 3.72, and 3.73 cm² for patient A, B, C and D respectively. Minimum distances between implanted TAVI device and coronary arteries (right and left) after the deflation of the balloon were 10.9, 11.4, 10.5, and 5.5 mm for patient A, B, C and D respectively, with no direct obstruction of the ostia.

In all cases, the virtual implantation of the TAVI device predicted a successful procedural outcome with an orifice area larger than the pre-implantation stenotic area, and no interference with other cardiac structures. Furthermore, patient-specific FE analyses showed no fractures of the stent immediately post-implantation. These methodologies might help engineers to better understand the mechanical behaviour of the stent when interacting with a wide variety of potential anatomies and, therefore, to optimise the device design for different potential clinical applications before actual procedures are performed.

3.2 Patients with aortic incompetence

A patient (E) diagnosed with congenital, moderate aortic valve stenosis, which was treated after birth with aortic balloon valvuloplasty, was selected. At 21 years of age, this patient was referred for surgical repair of her severe aortic valve regurgitation. FE model of TAVI in this patient specific native aortic root and valve leaflets was performed using the same TAVI stent model described above.

CT image data (CT-SOMATOM Definition) from the patient corresponding to mid-systole (i.e. open aortic valve leaflets) were elaborated in the image post-processing software Mimics. A 3D model of the aortic root, coronary arteries and valve leaflets was obtained for the patient (Fig. 17). The native structures were meshed with 3D triangular shell general-purpose elements (18,890 elements). Aortic wall and native valve leaflets were assumed to be respectively 2 and 0.5 mm thick (Conti et al., 2010) with density equal to 1,120 kg/m³, and Mooney-Rivlin hyperelastic constitutive law was adopted to describe the material behaviour.

In model E, the TAVI stent/balloon was placed in 3 different positions within the aortic root to test the influence of the landing zone into safe anchoring, the interference with other cardiac structures, such as the mitral valve and the atrioventricular node, and potential occlusion of the coronary arteries. First, the central section of the stent was placed aligned to the leaflet commissures (E_M; Fig 17), then it was moved 4.2 mm proximally towards the left ventricle (E_P; Fig. 17), and 4.2 mm distally towards the aortic arch (E_D; Fig. 17).

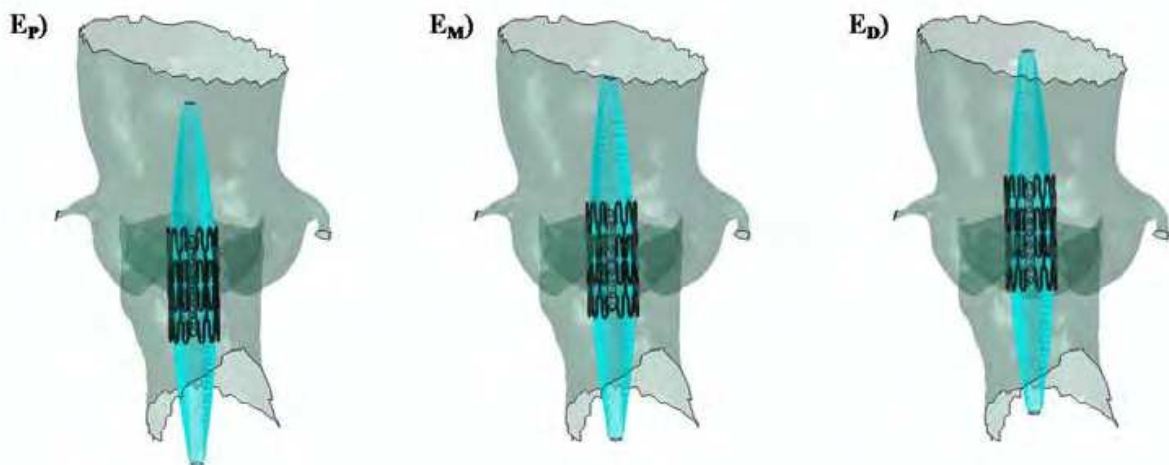


Fig. 17. Balloon and TAVI stent in the 3 analysed positions inside the native aortic valve: in correspondence of the leaflet commissures (E_M); moved 4.2 mm proximally towards the left ventricle (E_P); and, 4.2 mm distally towards the aortic arch (E_D).

The same loading and boundary conditions as those described above for the study of TAVI in bioprosthetic valves were adopted. Also, the same quantities of interests were measured.

In this patient, at the end of stent deployment and balloon deflation, the device assumed an asymmetrical configuration for all tested positions, more open distally than proximally (Fig. 18). In all 3 cases, the interaction between the TAVI device and the native implantation site was well confined within the left ventricular outflow tract and aortic root portion of the patient's morphology, thus reducing the potential risk of heart block and mitral valve leaflet entrapment. The stent implanted in this patient in the most distal position was the closest to the right coronary artery (3.1 mm). The TAVI device caused no direct obstruction of the coronary orifice; however, further fluid-dynamic studies could enhance our understanding of the effects of the TAVI device placement to the coronary flow.

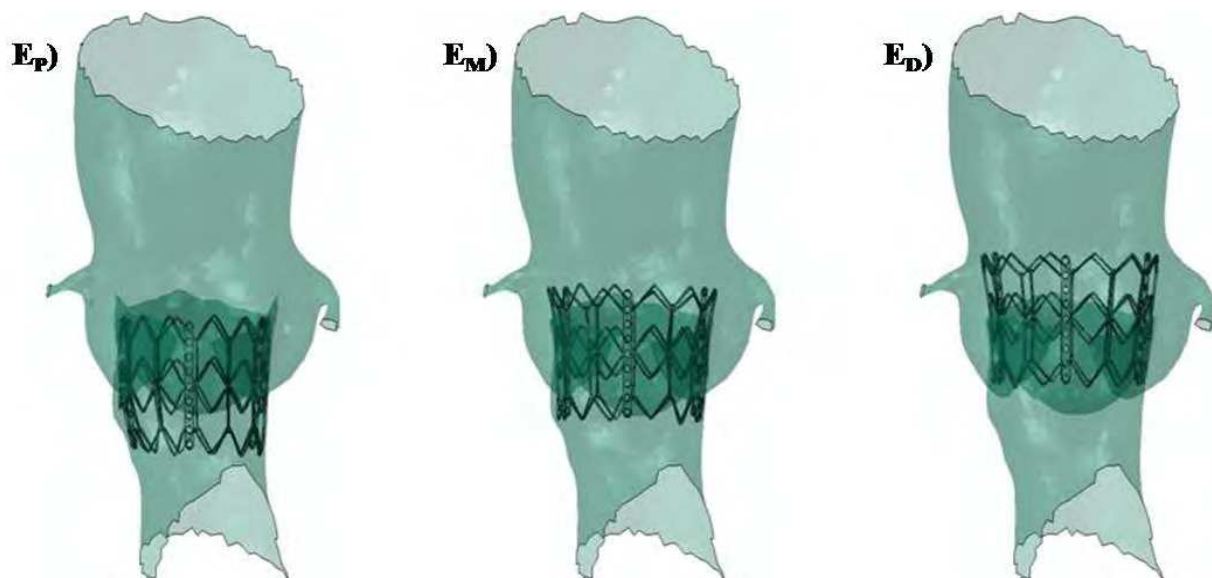


Fig. 18. TAVI stent final configuration (end of balloon deflation) in the 3 simulated positions.

At balloon deflation, the interaction with the native aortic valve and wall caused high recoil in the proximal section of the stent for all 3 tested positions $E_M = 14.9\%$; model $E_P = 20.2\%$; model $E_D = 11.4\%$. This may be considered a potential cause for obstruction of the left ventricular outflow tract and result in potential dislodgment of the TAVI device from its original position. However, the final geometric orifice areas for the analysed patient in the 3 positions E_M , E_P , and E_D – 4.7, 3.7 and 5.3 cm^2 respectively – were same size or larger than the initial orifice area = 3.7 cm^2 .

Direct interaction of TAVI stent with native tissue had impacts both on the device and on the implantation site. After recoil, the geometrical configuration of the stent was not uniform, with an asymmetrical stress distribution (max 477 MPa for E_P). The ultimate stress value for the stent material (stainless steel AISI 316L ultimate strength = 515 MPa) was not reached; this means that no stent fractures were seen immediately after deployment. However, pulsatile compressions during cardiac cycle could affect the long-term performance of this stent due to the dynamic nature of the native, non-calcified implantation site. This may be particularly relevant for model E_P where the distal portion of the device was in direct contact with the active muscular portion of the left ventricular outflow tract.

The expansion of the TAVI stent within native tissue also caused high maximum principal stresses (1 MPa) in the arterial wall, in particular in the region of the leaflets for model E_D , at commissure level (Fig. 19). This might induce damage or stimulate remodelling (e.g. stenosis).

A careful balance between interrelated and sometimes contradictory requirements has to be achieved for optimal TAVI positioning and outcomes such as relief of valve dysfunction and safe anchoring with no tissue damage, no coronary obstruction, no interference with other cardiac structures and no device failure in both short- and long-term. Patient specific FE analysis can be used to help in this process of optimisation and represent an additional assessment tool for the selection of patients for TAVI.

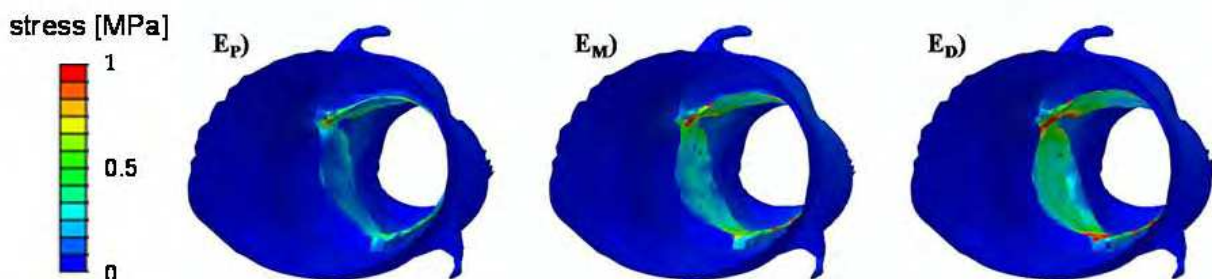


Fig. 19. Maximum principal stress distribution in the native aortic valve leaflets and aortic root after balloon deflation in models E_P , E_M and E_D .

4. Conclusion

Engineering and computational methodologies, together with state of the art imaging technologies, can be used to replicate patient specific patho-physiological conditions in virtual models. Combining patient specific imaging data and computational modelling can improve our understanding of heart structures and the way devices interact with them.

Therefore, advanced FE analyses can become a fundamental tool during preclinical testing of new biomedical devices that could shorten the time for device development, minimise animal experimentation, and ensure greater patient safety during the delicate phase of testing clinical feasibility of novel cardiovascular technologies.

5. Acknowledgements

This work has been supported by grant funding from the British Heart Foundation (BHF) (Dr. Schievano & Mr. Capelli – PhD Studentships), the Royal Academy of Engineering and the Engineering and Physical Sciences Research Council (EPSRC) (Dr. Schievano – Post-doctoral Fellowship), the National Institute of Health Research (NIHR) (Professor Taylor – Senior Research Fellowship), the European Union (Ms. Cosentino – MeDDiCA PhD Studentship 7th Framework Programme, grant agreement 238113) and the Fondation Leducq.

6. References

- Beden, S.M., Abdullah, S., Ariffin, A.K., AL-Asady, N.A., & Rahman, M.M. (2009). Fatigue life assessment of different steel-based shell materials under variable amplitude loading. *European Journal of Scientific Research*, Vol.29, No.1, pp. 157-169
- Bonhoeffer, P., Boudjemline, Y., Saliba, Z., Merckx, J., Aggoun, Y., Bonnet, D., Acar, P., Le Bidois, J., Sidi, D., & Kachaner, J. (2000). Percutaneous replacement of pulmonary valve in a right-ventricle to pulmonary-artery prosthetic conduit with valve dysfunction. *Lancet*, Vol.356, No.9239, (21 October 2000), pp. 1403-1405
- Bonhoeffer, P., Huynh, R., House, M., Douk, N., Kopcak, M., Hill, A., & Rafiee, N. (2008). Transcatheter pulmonic valve replacement in sheep using a grafted self-expanding stent with tissue valve. *Circulation*. Vol.118, pp. S_812
- Bosi, G.M., Cerri, E., Capelli, C., Migliavacca, F., Bonhoeffer, P., Taylor, A.M., & Schievano, S. (2010). Patient-specific study of transcatheter aortic valve implantation. Endocoronary Biomechanics Research Symposium, Marseille, France, May 2010
- Capelli, C., Taylor, A.M., Migliavacca, F., Bonhoeffer, P., & Schievano, S. (2010a). Patient-specific reconstructed anatomies and computer simulations are fundamental for selecting medical device treatment: application to a new percutaneous pulmonary valve. *Philosophical Transactions of the Royal Society A: Mathematical, Physical and Engineering Sciences*, Vol.368, No.1921, (28 June 2010), pp. 3027-3038
- Capelli, C., Nordmeyer, J., Schievano, S., Lurz, P., Khambadkone, S., Lattanzio, S., Taylor, A.M., Petrini, L., Migliavacca, F., & Bonhoeffer, P. (2010b). How do angioplasty balloons work: a computational study on balloon expansion forces. *EuroIntervention*, Vol.6, No.5, (November 2010), pp. 638-642
- Cribier, A., Eltchaninoff, H., Bash, A., Borenstein, N., Tron, C., Bauer, F., Derumeaux, G., Anselme, F., Laborde, F., & Leon, M.B. (2002). Percutaneous transcatheter implantation of an aortic valve prosthesis for calcific aortic stenosis - first human case description. *Circulation*, Vol.106, No.24, (10 December 2002), pp. 3006-3008
- Cribier, A. (2009). Transcatheter Aortic Valve Implantation: What are the perspectives? at Innovations in Cardiovascular Interventions (ICI) Meeting 2009.
http://www.paragon-conventions.net/ICI_PDF/Alain%20Cribier.pdf

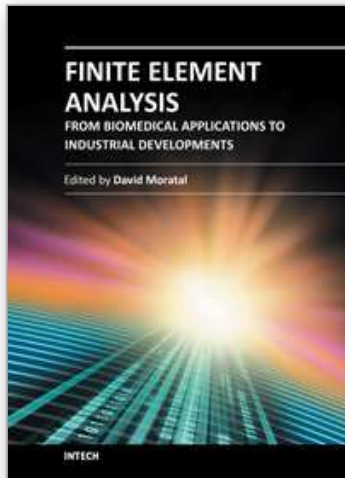
- Conti, C.A., Votta, E., Della Corte, A., Del Viscovo, L., Bancone, C., Cotrufo, M., & Redaelli, A. (2010). Dynamic finite element analysis of the aortic root from MRI-derived parameters. *Medical Engineering & Physics*, Vol.32, No.2, (March 2010), pp. 212-221
- Cosentino, D., Capelli, C., Pennati, G., Díaz-Zuccarini, V., Bonhoeffer, P., Taylor, A.M., Schievano, S. (2011). Stent Fracture Prediction in Percutaneous Pulmonary Valve Implantation: A Patient-Specific Finite Element Analysis. *International Conference on Advancements of Medicine and Health Care through Technology, IFMBE Proceedings*, Vol.36, Part 4, (01 January 2011), pp. 288-293
- De Beule, M., Mortier, P., Carlier, S.G., Verheghe, B., Van Impe, R., & Verdonck, P. (2008). Realistic finite element-based stent design: The impact of balloon folding. *Journal of Biomechanics*, Vol.41, No.2, pp. 383-389
- Delgado, V., Ewe, S.H., Ng, A.C.T., van der Kley, F., Marsan, N.A., Schuijf, J.D., Schaliij, M.J., & Bax, J.J. (2010) Multimodality imaging in transcatheter aortic valve implantation: Key steps to assess procedural feasibility. *Eurointervention*, Vol.6, No.5 (November 2010), pp. 643-652
- Gervaso, F., Capelli, C., Petrini, L., Lattanzio, S., Di Virgilio, L., & Migliavacca, F. (2008). On the effects of different strategies in modelling balloon-expandable stenting by means of finite element method. *Journal of Biomechanics*, Vol.41, No.6, pp. 1206-1212
- Lee, J.M., Boughner, D. R., & Courtman, D.W. (1984). The glutaraldehyde-stabilized porcine aortic-valve xenograft .2. Effect of fixation with or without pressure on the tensile viscoelastic properties of the leaflet material. *Journal of Biomedical Materials Research*, Vol.18, No.1, (January 1984), pp. 79-98
- Leon, M.B., Piazza, N., Nikolsky, E., Blackstone, E.H., Cutlip, D.E., Kappetein, A.P., Krucoff, M.W., Mack, M., Mehran, R., Miller, C., Morel, M.A., Petersen, J., Popma, J.J., Takkenberg, J.J.M., Vahanian, A., van Es, G.A., Vranckx, P., Webb, J.G., Windecker, S., & Serruys, P.W. (2011). Standardized endpoint definitions for transcatheter aortic valve implantation clinical trials a consensus report from the valve academic research consortium. *Journal of the American College of Cardiology*, Vol.57, No.3, (18 January 2011), pp. 253-269
- Loree, H.M., Grodzinsky, A.J., Park, S.Y., Gibson, L.J., Lee, R.T. (1994). Static circumferential tangential modulus of human atherosclerotic tissue. *Journal of Biomechanics*, Vol.27, No.2, (February 1994), pp. 195-204
- Lurz, P., Coats, L., Khambadkone, S., Boudjemline, Y., Schievano, S., Muthurangu, V., Lee, T.Y., Parenzan, G., Derrick, G., Cullen, S., Walker, F., Tsang, V., Deanfield, J., Taylor, A.M., & Bonhoeffer, P. (2008). Percutaneous pulmonary valve implantation - Impact of evolving technology and learning curve on clinical outcome. *Circulation*, Vol.117, No.15, (15 April 2008), pp. 1964-1972
- Marrey, R.V., Burgermeister, R., Grishaber, R.B., & Ritchie, R.O. (2006). Fatigue and life prediction for cobalt-chromium stents: a fracture mechanics analysis. *Biomaterials*, Vol.27, No.9, (March 2006), pp. 1988-2000
- McElhinney, D.B., Hellenbrand, W.E., Zahn, E.M., Jones, T.K., Cheatham, J.P., Lock, J.E., & Vincent, J.A. (2010). Short- and medium-term outcomes after transcatheter pulmonary valve placement in the expanded multicenter US melody valve trial. *Circulation*, Vol.122, No.5, (3 August 2010), pp. 507-516
- Migliavacca, F., Baker, C., Biglino, G., Bosi, G., Capelli, C., Cerri, E., Corsini, C., Cosentino, D., Hsia, T.Y., Pennati, G., & Schievano, S. (2011). Numerical simulations to study

- aortic arch pathologies: application to hypoplastic left heart syndrome, aortic coarctation and aortic valve diseases. In "New endovascular technologies: from bench test to clinical practice". Eds. Chakfé N, Durand B and Meichelboeck W. Europrot, Strasbourg, France, 9-22, 2011
- Nordmeyer, J., Khambadkone, S., Coats, L., Schievano, S., Lurz, P., Parenzan, G., Taylor, A.M., Lock, J.E., & Bonhoeffer, P. (2007). Risk stratification, systematic classification and anticipatory management strategies for stent fracture after percutaneous pulmonary valve implantation. *Circulation*, Vol.115, No.11 (20 March 2007), pp. 1392-1397
- Nordmeyer, J., Coats, L., Lurz, P., Lee, T.Y., Derrick, G., Rees, P., Cullen, S., Taylor, A.M., Khambadkone, S., & Bonhoeffer, P. (2008). Percutaneous pulmonary valve-in-valve implantation: a successful treatment concept for early device failure. *European Heart Journal*, Vol. 29, No.6 (March 2008), pp. 810-815
- Nordmeyer, J., Lurz, P., Khambadkone, S., Schievano, S., Jones, A., McElhinney, D.B., Taylor, A.M., & Bonhoeffer, P. (2011). Pre-stenting with a bare metal stent before percutaneous pulmonary valve implantation: Acute and one-year outcomes. *Heart*, Vol.97, No.2, (January 2011), pp. 118-123
- Okamoto, R., Wagenseil, J.E., DeLong, W.R., Peterson, S.J., Kouchoukos, N.T., & Sundt, T.M. (2002). Mechanical Properties of Dilated Human Ascending Aorta. *Annals of Biomedical Engineering*, Vol.30 No.5, (May 2002), pp. 624-635
- Petrini, L., Migliavacca, F., Massarotti, P., Schievano, S., Dubini, G., & Auricchio, F. (2005). Computational studies of shape memory alloy behavior in biomedical applications. *Journal of Biomechanical Engineering*, Vol.127, No.4 (August 2005), pp. 716-725
- Rodes-Cabau, J., Webb, J.G., Cheung, A., Ye, J., Dumont, E., Feindel, C.M., Osten, M., Natarajan, M.K., Velianou, J.L., Martucci, G., DeVarenes, B., Chisholm, R., Peterson, M.D., Lichtenstein, S.V., Nietlispach, F., Doyle, D., DeLarochelliere, R., Teoh, K., Chu, V., Dancea, A., Lachapelle, K., Cheema, A., Latter, D., & Horlick, E. (2010). Transcatheter aortic valve implantation for the treatment of severe symptomatic aortic stenosis in patients at very high or prohibitive surgical risk acute and late outcomes of the multicenter canadian experience. *Journal of the American College of Cardiology*, Vol.55, No.11, (16 March 2010), pp. 1080-1090
- Schievano, S.; Coats, L.; Migliavacca, F.; Norman, W.; Frigiola, A.; Deanfield, J.; Bonhoeffer, P., & Taylor, A.M. (2007a). Variations in right ventricular outflow tract morphology following repair of congenital heart disease: implications for percutaneous pulmonary valve implantation. *Journal of cardiovascular magnetic resonance*, Vol.9, No.4, (February 2007), pp. 687-695
- Schievano, S.; Migliavacca, F.; Coats, L.; Khambadkone, S.; Carminati, M.; Wilson, N.; Deanfield, J.E.; Bonhoeffer, P., & Taylor, A.M. (2007b). Percutaneous pulmonary valve implantation based on rapid prototyping of right ventricular outflow tract and pulmonary trunk from MR data. *Radiology*, Vol.242, No.2, (February 2007), pp. 490-497
- Schievano, S., Petrini, L., Migliavacca, F., Coats, L., Nordmeyer, J., Lurz, P., Khambadkone, S., Taylor, A.M., Dubini, G., & Bonhoeffer, P. (2007c). Finite element analysis of stent deployment: understanding stent fracture in percutaneous pulmonary valve implantation. *Journal Interventional Cardiology*, Vol.20, No.6, (December 2007), pp. 546-554

- Schievano, S., Kunzelman, K., Nicosia, M.A., Cochran, R.P., Einstein, D.R., Khambadkone, S., & Bonhoeffer, P. (2009). Percutaneous mitral valve dilatation: single balloon versus double balloon. A finite element study. *Journal of Heart Valve Disease*, Vol.18, No.1, (January 2009), pp. 28-34
- Schievano, S.; Taylor, A.M.; Capelli, C.; Coats, L.; Walker, F.; Lurz, P.; Nordmeyer, J.; Wright, S.; Khambadkone, S.; Tsang, V.; Carminati, M., & Bonhoeffer, P. (2010a). First-in-man implantation of a novel percutaneous valve: a new approach to medical device development. *Eurointervention*, Vol.5, No.6, (January 2010), pp. 745-750
- Schievano, S., Taylor, A.M., Capelli, C., Lurz, P., Nordmeyer, J., Migliavacca, F., & Bonhoeffer, P. (2010b). Patient specific finite element analysis results in more accurate prediction of stent fractures: Application to percutaneous pulmonary valve implantation. *Journal of Biomechanics*, Vol.43, No.4, (3 March 2010), pp. 687-93
- Schievano, S., Capelli, C., Young, C., Lurz, P., Nordmeyer, J., Owens, C., Bonhoeffer, P., & Taylor, A.M. (2011). Four-dimensional computed tomography: a method of assessing right ventricular outflow tract and pulmonary artery deformations throughout the cardiac cycle. *European Radiology*, Vol.21, No.1, (January 2011), pp. 36-45
- Schoenhagen, P., Hill, A., Kelley, T., Popovic, Z., & Halliburton, S.S. (2011). In vivo imaging and computational analysis of the aortic root. Application in clinical research and design of transcatheter aortic valve systems. *Journal of Cardiovascular Translational Research*, Vol.4, No. 4, (August 2011), pp. 459-469
- Sines, G., & Ohgi, G. (1981). Fatigue criteria under combined stresses or strains. *Journal of Engineering Materials and Technology*, Vol.103, No.2, (April 1981), pp. 82-90
- Smith, C.R., Leon, M.B., Mack, M.J., Miller, D.C., Moses, J.W., Svensson, L.G., Tuzcu, E.M., Webb, J.G., Fontana, G.P., Makkar, R.R., Williams, M., Dewey, T., Kapadia, S., Babaliaros, V., Thourani, V.H., Corso, P., Pichard, A.D., Bavaria, J.E., Herrmann, H.C., Akin, J.J., Anderson, W.N., Wang, D., Pocock, S.J., & Investigators PT (2011) Transcatheter versus surgical aortic-valve replacement in high-risk patients. *New England Journal of Medicine*, Vol.364, No.23, (9 June 2011), pp. 2187-2198
- Taylor, C.A., & Figueroa, C.A. (2009). Patient-specific modeling of cardiovascular mechanics. *Annual Review of Biomedical Engineering*, Vol.11, pp. 109-134
- Ussia, G.P., Mulè, M., Barbanti, M., Cammalleri, V., Scarabelli, M., Immè, S., Capodanno, D., Ciriminna, S., & Tamburino, C. (2009). Quality of life assessment after percutaneous aortic valve implantation. *European Heart Journal*, Vol.30, No.14, (July 2009), pp. 1790-1796
- Vahanian, A., Alfieri, O., Al-Attar, N., Antunes, M., Bax, J., Cormier, B., Cribier, A., De Jaegere, P., Fournial, G., Kappetein, A.P., Kovac, J., Ludgate, S., Maisano, F., Moat, N., Mohr, F., Nataf, P., Piérard, L., Pomar, J.L., Schofer, J., Tornos, P., Tuzcu, M., van Hout, B., Von Segesser, L.K., Walther, T. & European Association of Cardio-Thoracic Surgery; European Society of Cardiology; European Association of Percutaneous Cardiovascular Interventions. (2008). Transcatheter valve implantation for patients with aortic stenosis: a position statement from the European Association of Cardio-Thoracic Surgery (EACTS) and the European Society of Cardiology (ESC), in collaboration with the European Association of

- Percutaneous Cardiovascular Interventions (EAPCI). *European Heart Journal*, Vol.29, No.11, (June 2008), pp. 1463-1470
- Walther, T., Dehdashtian, M.M., Khanna, R., Young, E., Goldbrunner, P.J., & Lee, W. (2011). Trans-catheter valve-in-valve implantation: in vitro hydrodynamic performance of the SAPIEN+cloth trans-catheter heart valve in the Carpentier-Edwards Perimount valves. *European Journal of Cardio-thoracic Surgery*, Vol.40, No.5, (November 2011), pp. 1120-1126
- Webb, J.G., Wood, D.A., Ye, J., Gurvitch, R., Masson, J.B., Rodés-Cabau, J., Osten, M., Horlick, E., Wendler, O., Dumont, E., Carere, R.G., Wijesinghe, N., Nietlispach, F., Johnson, M., Thompson, C.R., Moss, R., Leipsic, J., Munt, B., Lichtenstein, S.V., & Cheung, A. (2010). Transcatheter valve-in-valve implantation for failed bioprosthetic heart valves. *Circulation*, Vol.121, No.16, (27 April 2010), pp. 1848-1857
- Zajarias, A., & Cribier, A.G. (2009). Outcomes and safety of percutaneous aortic valve replacement. *Journal of the American College of Cardiology*, Vol.53, No.20, (19 May 2009), pp. 1829-1836
- Zioupos, P., Barbenel, J.C., & Fisher, J. (1994). Anisotropic elasticity and strength of glutaraldehyde fixed bovine pericardium for use in pericardial bioprosthetic valves. *Journal of Biomedical Materials Research*, Vol.28, No. 1, (January 1994), pp. 49-57

IntechOpen



Finite Element Analysis - From Biomedical Applications to Industrial Developments

Edited by Dr. David Moratal

ISBN 978-953-51-0474-2

Hard cover, 496 pages

Publisher InTech

Published online 30, March, 2012

Published in print edition March, 2012

Finite Element Analysis represents a numerical technique for finding approximate solutions to partial differential equations as well as integral equations, permitting the numerical analysis of complex structures based on their material properties. This book presents 20 different chapters in the application of Finite Elements, ranging from Biomedical Engineering to Manufacturing Industry and Industrial Developments. It has been written at a level suitable for use in a graduate course on applications of finite element modelling and analysis (mechanical, civil and biomedical engineering studies, for instance), without excluding its use by researchers or professional engineers interested in the field, seeking to gain a deeper understanding concerning Finite Element Analysis.

How to reference

In order to correctly reference this scholarly work, feel free to copy and paste the following:

Silvia Schievano, Claudio Capelli, Daria Cosentino, Giorgia M. Bosi and Andrew M. Taylor (2012). Finite Element Analysis to Study Percutaneous Heart Valves, Finite Element Analysis - From Biomedical Applications to Industrial Developments, Dr. David Moratal (Ed.), ISBN: 978-953-51-0474-2, InTech, Available from: <http://www.intechopen.com/books/finite-element-analysis-from-biomedical-applications-to-industrial-developments/finite-element-analysis-to-study-percutaneous-heart-valves>

INTECH
open science | open minds

InTech Europe

University Campus STeP Ri
Slavka Krautzeka 83/A
51000 Rijeka, Croatia
Phone: +385 (51) 770 447
Fax: +385 (51) 686 166
www.intechopen.com

InTech China

Unit 405, Office Block, Hotel Equatorial Shanghai
No.65, Yan An Road (West), Shanghai, 200040, China
中国上海市延安西路65号上海国际贵都大饭店办公楼405单元
Phone: +86-21-62489820
Fax: +86-21-62489821

© 2012 The Author(s). Licensee IntechOpen. This is an open access article distributed under the terms of the [Creative Commons Attribution 3.0 License](#), which permits unrestricted use, distribution, and reproduction in any medium, provided the original work is properly cited.

IntechOpen

IntechOpen